JACS
JOURNAL OF THE AMERICAN CHEMICAL SOCIETY

Article

pubs.acs.org/JACS

Proximal Ligand Electron Donation and Reactivity of the Cytochrome P450 Ferric–Peroxo Anion

Santhosh Sivaramakrishnan,[†] Hugues Ouellet,[†,‡] Hirotoshi Matsumura,[§] Shenheng Guan,[†] Pierre Moënne-Loccoz,[§] Alma L. Burlingame,[†] and Paul R. Ortiz de Montellano*[,†]

[†]Department of Pharmaceutical Chemistry, University of California, 600 16th Street, San Francisco, California 94158-2517, United States

[§]Division of Environmental & Biomolecular Systems, Oregon Health & Science University, 20,000 NW Walker Road, Beaverton, Oregon 97006-8921, United States

Supporting Information

ABSTRACT: CYP125 from *Mycobacterium tuberculosis* catalyzes sequential oxidation of the cholesterol side-chain terminal methyl group to the alcohol, aldehyde, and finally acid. Here, we demonstrate that CYP125 simultaneously catalyzes the formation of five other products, all of which result from deformylation of the sterol side chain. The aldehyde intermediate is shown to be the precursor of both the conventional acid metabolite and the five deformylation products. The acid arises by protonation of the ferric–peroxo anion species and formation of the ferryl–oxene species, also known as Compound I, followed by hydrogen abstraction and oxygen transfer. The deformylation products arise by addition of the same ferric–peroxo anion to the aldehyde intermediate to give a peroxyhemiacetal that leads to C–C bond cleavage. This bifurcation of the catalytic sequence has allowed us to examine the effect of electron donation by the proximal ligand on the properties of the ferric–peroxo anion. Replacement of the cysteine thiolate iron ligand by a selenocysteine results in UV–vis, EPR, and resonance Raman spectral changes indicative of an increased electron donation from the proximal selenolate ligand to the iron. Analysis of the product distribution in the reaction of the selenocysteine substituted enzyme reveals a gain in the formation of the acid (Compound I pathway) at the expense of deformylation products. These observations are consistent with an increase in the pK_a of the ferric–peroxo anion, which favors its protonation and, therefore, Compound I formation.

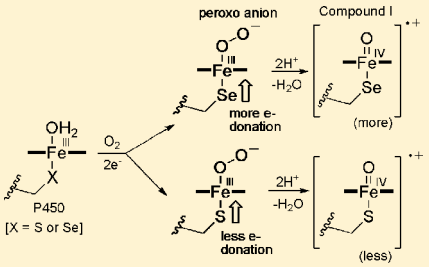

INTRODUCTION

The cytochromes P450 (CYPs) are heme–thiolate enzymes that use O_2 and two reducing equivalents to insert an oxygen atom into organic compounds, including fatty acids, steroids, and xenobiotics. CYPs have been identified in all domains of life and more than 11 500 distinct isoforms are now known.[1] In humans, some CYPs, (e.g., CYP19 or CYP51) are highly specific and act on a single substrate, or a few closely related substrates, whereas other isoforms (e.g., CYP3A4, CYP2D6 and CYP2C9) are promiscuous and are responsible for the oxidation of approximately 70% of all therapeutic drugs.[2] In contrast, the biological function(s) of the vast majority of bacterial CYPs remain to be elucidated, but some (e.g., EryF, EpoK, OxyB, OxyD, PikC, and PimD) have been shown to be involved in the biosynthesis of antibiotics.[3−12] Other bacterial CYPs have been shown to participate in catabolic pathways, including the degradation of terpenoids (e.g., CYP176A1 ($P450_{cin}$),[13] steroids (CYP125 and CYP142),[14−19] and explosives (XplA).[20,21]

The P450 catalytic cycle is initiated by one electron reduction of the ferric heme iron (Fe^{3+}) to the ferrous state (Fe^{2+}) which then binds molecular oxygen to give the ferrous dioxy (Fe^{2+}-O_2) form. A second electron transfer to this intermediate generates a ferric–peroxo anion (Fe^{3+}-O-O^-) that is converted by protonation to a ferric–hydroperoxo (Fe^{3+}-OOH) species named Compound 0. A second protonation of the distal oxygen of Compound 0 results in immediate fragmentation to give a molecule of water and a ferryl Fe^{4+}=O species with a radical cation delocalized over the porphyrin and the proximal thiolate iron ligand.[22] On the basis of peroxidase nomenclature, this intermediate can be designated as Compound I. In a conventional hydroxylation, Compound I abstracts a hydrogen atom from a substrate to give a carbon radical and the equivalent of an iron-bound hydroxyl radical, which then undergo radical recombination to give the hydroxylated product.[23,24] The factors governing the formation and stability of Compound I have been extensively studied.[25]

The cysteine thiolate ligated to the heme iron atom is believed to be important for the formation from molecular oxygen and reactivity of Compound I in cytochromes P450.[26] This feature distinguishes P450 enzymes from peroxidases, catalases and other heme containing enzymes in which the proximal iron ligand is either a histidine nitrogen or a tyrosine hydroxyl. Electron donation from the proximal cysteine thiolate ligand is proposed to facilitate protonation of the distal O–O

Received: December 8, 2011
Published: March 23, 2012

Scheme 1. Partitioning of the Ferric−Peroxo Anion into the Compound I-Mediated Monooxygenation (a) and Peroxyhemiacetal-Mediated Deformylation (b) Pathways in the Oxidation of an Aldehyde

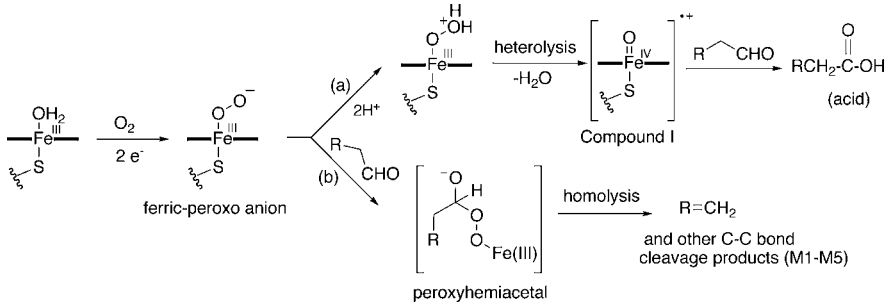

bond in Compound 0, thus, channeling this intermediate toward heterolytic formation of Compound I.[27,28]

Although Compound I is thought to be responsible for the majority of P450-catalyzed oxidations, it is not responsible for the oxidative C−C bond cleavage observed in the P450-mediated oxidation of aldehydes. Nucleophilic addition of the ferric−peroxo anion intermediate to the aldehyde to give a peroxyhemiacetal is the generally accepted key step in formation of the C−C bond cleavage products.[29−31] The actual C−C bond cleavage may occur by either concerted or homolytic radical fragmentation of the peroxyhemiacetal.[29] Thus, the ferric−peroxo anion intermediate can either undergo two protonation steps to generate Compound I, resulting in conventional monooxygenase activity, or it can add as a nucleophile to an aldehyde carbonyl group, triggering a reaction pathway that leads to C−C bond cleavage (Scheme 1). Although the effect of proximal electron donation on the reactivity and stability of Compound I has been studied, its impact on the reactions involving the ferric−peroxo anion intermediate remains obscure.

CYP125 from *Mycobacterium tuberculosis* (*Mtb*) is required for degradation[14,17−19] and incorporation of the cholesterol side chain into the lipidic virulence factor, phthiocerol dimycocerosate (PDIM).[19] In addition, CYP125 is also required to alleviate the toxic effect of cholest-4-en-3-one on *Mtb* growth in vitro.[19] CYP125 is a steroid C26-monooxygenase that sequentially oxidizes the terminal methyl of the side chain of both cholesterol and cholest-4-en-3-one to the alcohol, aldehyde, and finally carboxylic acid.[19] This same oxidation of cholesterol is catalyzed by two other enzymes from *Mtb*, CYP124 and CYP142,[17] and by the human enzyme CYP27A1.[32]

In this work, we have examined in greater detail the enzymatic activity of CYP125 with cholesterol and cholest-4-en-3-one. Liquid-chromatography mass spectrometry (LC−MS) in combination with deuterium- and $^{18}O_2$-labeling has led to the identification of five additional metabolites produced by this surprisingly versatile enzyme, all of which arise by carbon−carbon bond cleavage stemming from attack of the ferric−peroxo anion on the intermediate aldehyde. Furthermore, a proximal selenocysteine substituted CYP125, SeCYP125, was expressed, purified, and characterized using UV−vis, resonance Raman, and EPR spectroscopy. The selenocysteine substitution has made it possible to investigate the role of electron donation by the proximal ligand on partitioning between the reaction pathways that lead to formation of the carboxylic acid versus carbon−carbon bond cleavage. Our results provide direct evidence that increased proximal electron donation increases protonation of the ferric−peroxo anion, presumably by increasing its pK_a, and therefore promotes the formation of Compound I.

EXPERIMENTAL PROCEDURES

Materials. All solvents and reagents were of the highest purity commercially available unless noted otherwise. Methyl-β-cyclodextrin (mβCD), glucose-6-phosphate, glucose-6-phosphate dehydrogenase (*Saccharomyces cerevisiae*), ferredoxin (*Spinacea oleracea*), ferredoxin NADP$^+$-reductase (*S. oleracea*), cholesterol oxidase (*Streptomyces* sp.), cholesterol, cholest-4-en-3-one, progesterone and Dess-Martin reagent were purchased from Sigma-Aldrich (St. Louis, MO). (25*R*)-26-Hydroxycholesterol, (25*S*)-26-hydroxycholesterol and 1,4-cholestadiene-3-one were purchased from Research Plus (Barnegat, NJ). Cholest-4-en-3-one-(25*S*)-26-acid was obtained from Avanti Polar Lipids (Alabaster, AL).

Expression and Purification of CYP125$_{C173S/C429L}$ and SeCYP125$_{C173S/C429L}$. The C173S/C429L double mutant was used to eliminate all cysteine residues in the protein other than the proximal iron ligand. Amino acid substitution for the new construct CYP125$_{C173S/C429L}$ was carried out using a QuikChange site-directed mutagenesis kit (Stratagene) with the following primers: F_{C173S}, 5′-GTCGAGCAGGTTTCCTCTGAGCTGCCATTGCAG-3′; R_{C173S}, 5′-CTGCAATGGCAGCTCAGAGGAAACCTGCTCGAC-3′; F_{C429L}, 5′-CGACTACACCGGTAGACTCCCGGTTGCTCACT-3′; R_{C429L}, 5′-AGTGAGCAACCGGGAGTCTACCGGTGTAGTCG-3′. A construct in which the N-terminus was truncated at Val17 was used as a template. This construct was shown to improve crystallization and did not exhibit any difference in enzymatic activity. The mutations were verified using DNA sequencing. The CYP125 and CYP125$_{C173S/C429L}$ variant were purified as described previously.[19] The protein preparations were assayed for their P450 Fe^{2+}-CO difference spectrum and the concentration of P450 was determined from the difference spectrum using the extinction coefficient $\varepsilon_{450-490}$ = 91 000 mM^{-1} cm^{-1}.[33] No difference in stability or enzymatic activity was observed for the CYP125$_{C173S/C429L}$ variant relative to either the full-length or the truncated form of CYP125. Expression of the selenocysteine substituted CYP125$_{C173S/C429L}$, SeCYP125, was carried out according to the previously published protocol.[34] The enzyme was purified in the same way as the CYP125 protein[19] and the concentration was determined from the Fe^{2+}-CO difference spectrum using the extinction coefficient $\varepsilon_{459-490}$ = 91 000 mM^{-1} cm^{-1}. The total heme *b* content was also quantitated by the pyridine hemochrome method.[35] For clarity, the CYP125$_{C173S/C429L}$ containing cysteine at the active site and SeCYP125$_{C173S/C429L}$ proteins will be simply called WT* and SeCYP125, respectively.

EPR and Resonance Raman Spectroscopy. The EPR and resonance Raman (RR) analyses were performed with enzyme concentrations ranging from 40 to 100 μM. EPR spectra were obtained on a Bruker E500 X-band EPR spectrometer equipped with a superX microwave bridge and a dual mode cavity with a helium flow cryostat (ESR900, Oxford Instruments, Inc.). The microwave power, modulation amplitude, magnetic field sweep, and the sample temperature were optimized to ensure nonsaturating conditions for all low spin Fe^{3+} EPR active species. The RR spectra were collected

dx.doi.org/10.1021/ja211499q | J. Am. Chem. Soc. 2012, 134, 6673−6684

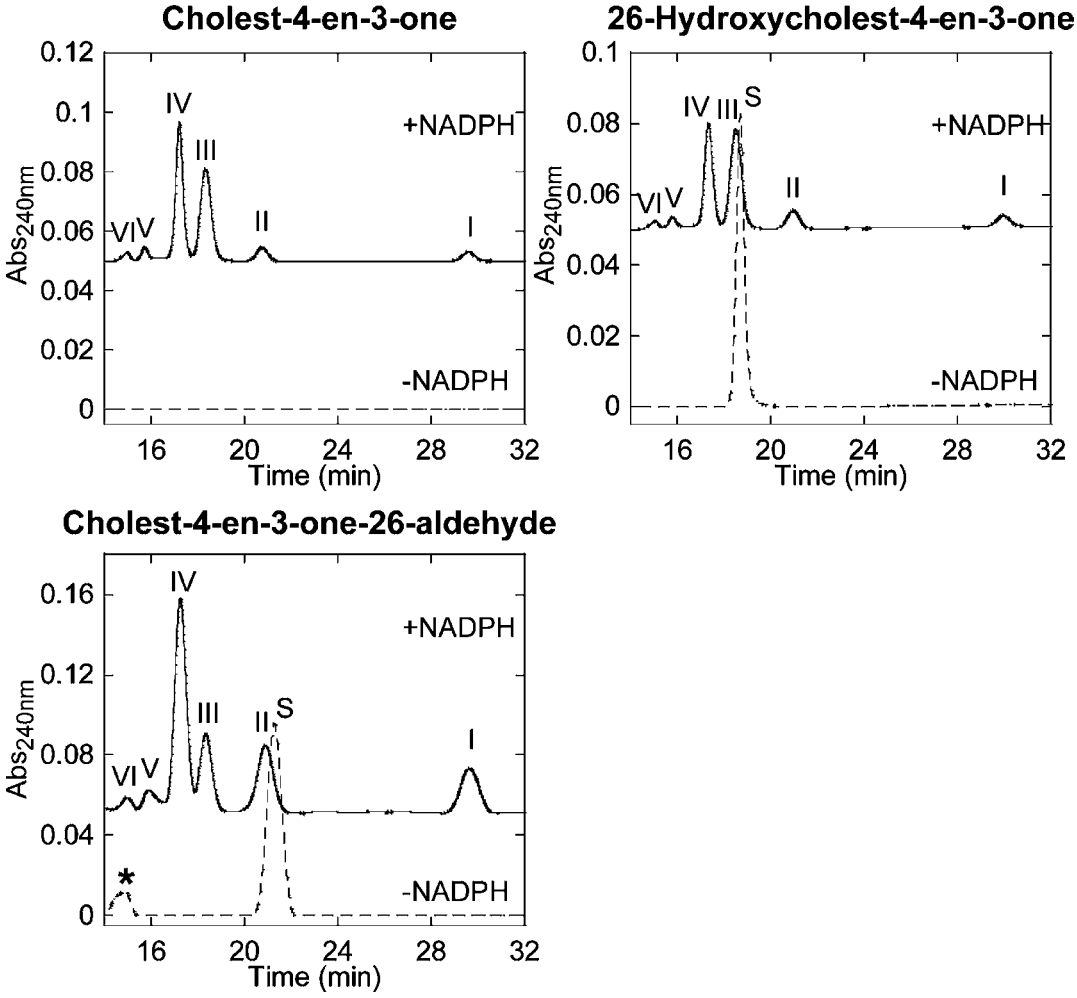

Figure 1. Reverse-phase HPLC separation of CYP125-catalyzed oxidation products of (A) cholest-4-en-3-one, (B) 26-hydroxycholest-4-en-3-one and (C) cholest-4-en-3-one-26-aldehyde. The separation of the products was carried out using a reverse phase C8-A Polaris column (Varian), as described in the Experimental Procedures. The elution was monitored at 240 nm. The retention times are: peak **VI**, 14.9 min; peak **V**, 15.8 min; peak **IV**, 17.2 min; peak **III**, 18.3 min; peak **II**, 20.8; peak **I**, 29.6 min. The m/z values of the parent and daughter ions are listed in Table S1. Asterisk (*) indicates contaminant from the cholest-4-en-3-one-26-aldehyde preparation.

using a 90° scattering geometry on room-temperature samples mounted on a reciprocating translation stage with a custom McPherson 2061/207 spectrograph (set at 0.67 m with variable gratings) equipped with a Princeton Instruments liquid-N_2-cooled CCD detector (LN-1100PB). The 413-nm excitation was obtained from an Innova 302 krypton laser (Coherent, Santa Clara CA) and the 442-nm excitation from a He/Cd laser (Liconix 4240NB). Kaiser Optical supernotch filters were used to attenuate Rayleigh scattering. Frequencies were calibrated relative to indene, CD_3CN and NO_g standards and are accurate to ± 1 cm^{-1}. Polarization conditions were optimized using CCl_4. The integrity of the RR samples, before and after illumination, was confirmed by direct monitoring of their UV−vis spectra in Raman capillaries.

Synthesis of Cholesterol-26-aldehyde. To a stirred solution of (25*S*)-26-hydroxy cholesterol (4.2 mg, 0.01 mmol) in CH_2Cl_2 (2 mL) was added Dess-Martin reagent (16 mg, 0.035 mmol). The resulting mixture was stirred at room temperature under an inert atmosphere for ~2 h. Diethyl ether (6 mL) was added and the reaction was quenched by the addition of NaOH (1N, 3 mL). The organic phase was separated, the aqueous phase was extracted with diethyl ether (3 × 5 mL), and the combined organic extracts were washed with NaOH (10 mL), water and brine solution. The resulting organic phase was dried over anhydrous Na_2SO_4, filtered and evaporated, giving an oil that was purified by preparative TLC (2% methanol in chloroform, R_f = 0.35) to yield ~2 mg (4.5 μmol, 45%) of the product. The identity of the product was confirmed by LC−MS analysis, which showed an m/z of 383 amu for the $[(M + H) - H_2O]^+$ ion. The presence of an aldehyde was further confirmed by a characteristic chemical shift at 9.6 ppm, corresponding to one aldehyde proton, in the ^1H NMR spectrum.

Enzyme Activity Assays. Substrate oxidation reactions were carried out in glass tubes at room temperature (23 °C) in 50 mM potassium phosphate buffer containing 0.05% (w/v) mβCD and 10 mM $MgCl_2$. In a typical 50 μL reaction, CYP125, WT*, or SeCYP125 (0.5 μM) was preincubated with the appropriate substrate (0.1 mM) for 5 min before the addition of spinach ferredoxin (1 μM), spinach ferredoxin-$NADP^+$ reductase (0.1 U/mL), bovine liver catalase (0.1 mg/mL), glucose-6-phosphate (4 mM), glucose-6-phosphate dehydrogenase (0.4 U/mL), and $NADP^+$ (0.1 mM). At appropriate time points, 50 μL aliquots of the reactions were quenched by the addition of 150 μL of acetonitrile containing 0.1% formic acid. The reaction mixtures were centrifuged at 11 000 rpm for 4 min and the supernatants were directly analyzed by LC−MS as described below. When necessary, cholesterol and other oxygenated cholesterol substrates were preincubated for 60 min at room temperature in the presence of 2.5 U/mL of cholesterol oxidase and 0.1 mg/mL of bovine liver catalase to convert the metabolites into their cholest-4-en-3-one derivatives. The UV−visible absorbance at 240 nm of the α, β-unsaturated ketone in cholest-4-en-3-one facilitates detection of the metabolites.

dx.doi.org/10.1021/ja211499q | *J. Am. Chem. Soc.* 2012, 134, 6673−6684

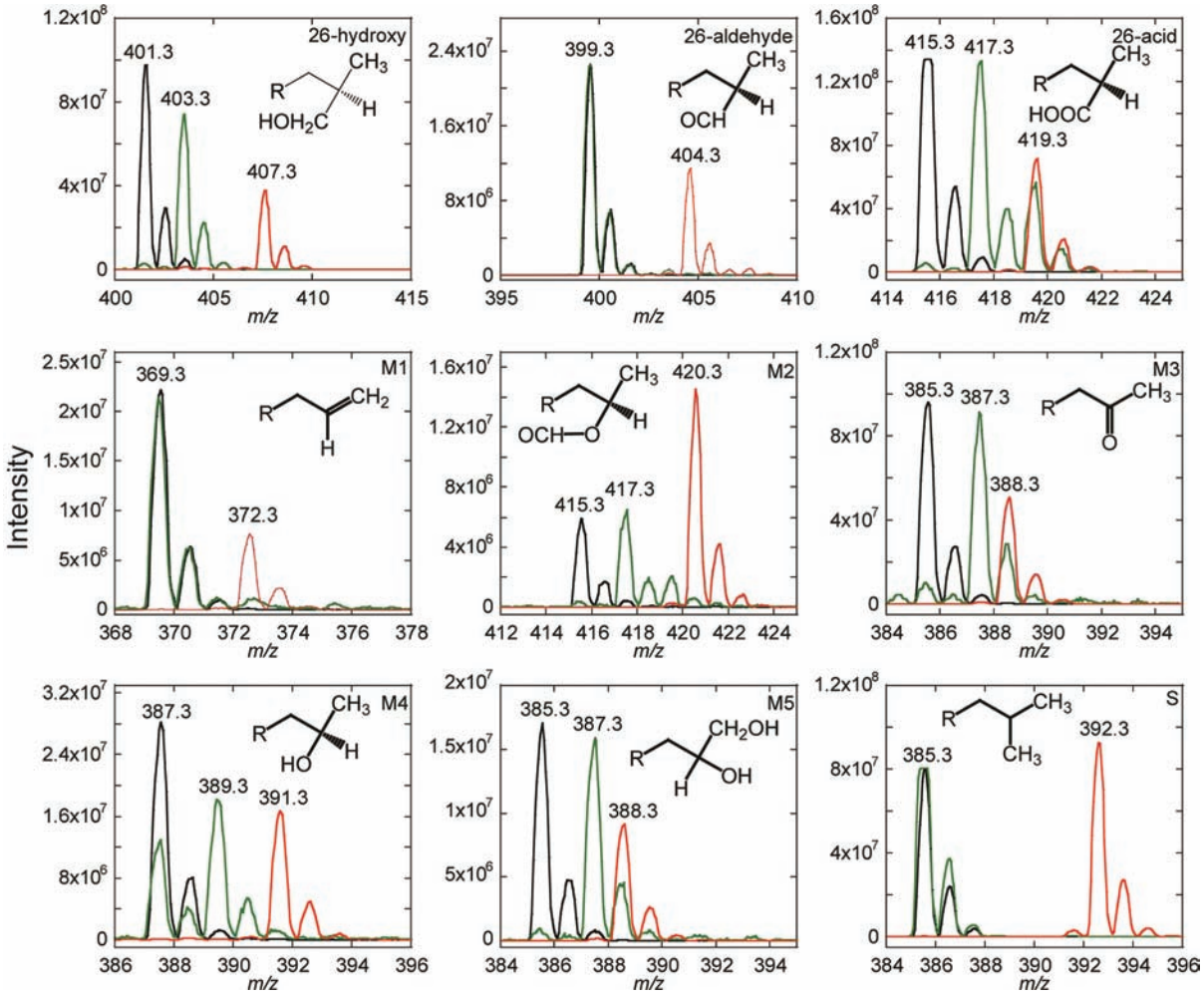

Figure 2. Mass spectra of the CYP125 oxidation products. Black trace, cholest-4-en-3-one under an atmosphere of $^{16}O_2$; green trace, cholest-4-en-3-one under an atmosphere of $^{18}O_2$; red trace; 25,26,26,26,27,27,27-d_7-cholest-4-en-3-one under an atmosphere of $^{16}O_2$. For clarity, only the m/z range showing the parent ion is presented. The proposed structures of the metabolites are also shown, where R represents the rest of the cholest-4-en-3-one structure.

Identification of Reaction Products by LC–MS. For qualitative analysis and identification of the metabolites, the reaction mixtures were analyzed by LC–MS using a Waters Micromass ZQ coupled to a Waters Alliance HPLC system equipped with a 2695 separations module, a Waters 2487 Dual λ Absorbance detector, and a reverse phase C8 column (Varian Polaris C8-A, 5 μm, 4.6 × 250 mm). The column was eluted isocratically at a flow rate of 0.5 mL/min (35% buffer A, H_2O + 0.1% formic acid (FA); 65% buffer B, CH_3CN + 0.1% FA). The elution was monitored at 240 nm. The mass spectrometer settings were as follows: mode, ES^+; capillary voltage, 3.5 kV; cone voltage, 25 V; desolvation temperature, 250 °C. The HPLC peaks of the individual metabolites were collected separately and analyzed by MS using a quadrupole instrument in the positive ion mode. The MS/MS analysis was performed at an Orbitrap XL instrument in the Higher Energy Collision Dissociation (HCD) mode.

For quantitation of the relative amounts of oxidation products, cholest-4-en-3-one (25 μM) was added as an internal standard for the oxidation of cholesterol, 26-hydroxycholesterol and cholesterol-26-aldehyde substrates. Similarly, 1,4-cholestadiene-3-one (25 μM) was added for the oxidation of cholest-4-en-3-one. The samples were analyzed by LC–MS as described above, but using a reverse phase C18 column (Waters Xterra C18 column, 3.5 μm, 2.1 × 50 mm). The contents were eluted at a flow rate of 0.5 mL/min (solvent A, H_2O + 0.1% formic acid (FA); solvent B, CH_3CN + 0.1% FA) with a gradient starting at 70% B up to 1 min and the solvents ramped up to 100% B over 12 min. The elution was maintained at 100% B up to 14 min and then ramped back to 70% B within 1 min, followed by equilibration at the same composition for 2 min before the next run. The cholesterol and its derivatives were analyzed using the total ion current signal obtained for the specific mass with selective ion monitoring. The starting materials showed a clear concentration dependent increase in the ion current signal. The individual metabolites were then quantitated as a ratio of the integrated ion current signal of the corresponding metabolite to the signal from the known concentration of the internal standard.

Enzyme Kinetics. The assays for determining the steady-state kinetic parameters were conducted as described above, but stopped at earlier time points to measure the initial rates. The reaction conditions were carefully optimized for the generation of a single product. All assays contained 0.25 μM of the corresponding enzyme in a final reaction volume of 300 μL, unless mentioned otherwise. For the first hydroxylation step, 0.45% of mβCD was used as reported before.[17] The kinetics for the second oxidation step was measured with 0.05% mβCD as reported above for the end-point assays.

RESULTS

Oxidative Activities of CYP125. We previously reported that the incubation of cholest-4-en-3-one with purified, recombinant *Mtb* CYP125, surrogate redox partners from spinach, and NADPH in the presence of 0.45% (w/v) mβCD resulted in the formation of three major products correspond-

dx.doi.org/10.1021/ja211499q | J. Am. Chem. Soc. 2012, 134, 6673–6684

Scheme 2. Possible Mechanisms for the Deformylation Reactions Catalyzed by CYP125[a]

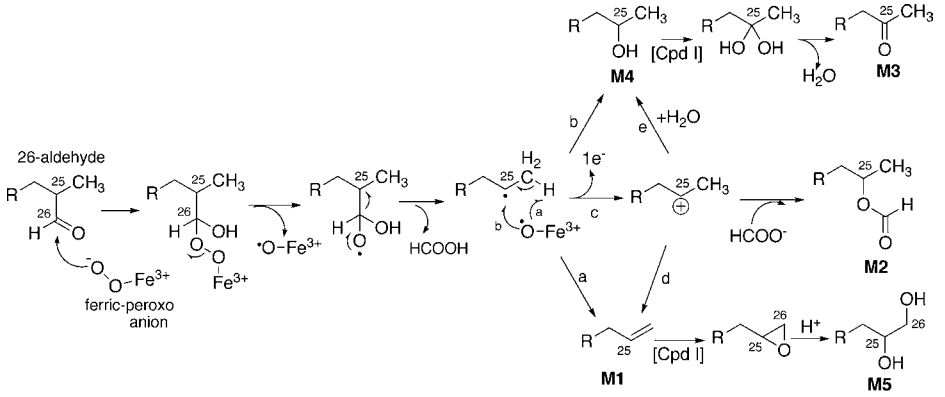

[a]The important steps involve addition of the ferric−peroxo anion of CYP125 to the C26 carbonyl and subsequent radical fragmentation of the peroxyhemiacetal adduct. The radical fragmentation of the peroxyhemiacetal adduct led to (a) the formation of an alkene (**M1**) or (b) the formation of a one-carbon deficient alcohol (**M4**). The Compound I-catalyzed oxidation of **M1** generates a diol (**M5**) via the acid-catalyzed ring-opening of an epoxide intermediate. A C25 cation may also derive from the single-electron oxidation of the C25 radical (c). Trapping of the cation by formate or water (e) results in the formation of the C25-oxyformyl (**M2**) and the one-carbon reduced alcohol (**M4**), respectively. Loss of a proton from the C25 cation may also generate M1 (d). The Compound I-catalyzed oxidation of **M4** produces a *gem*-diol intermediate that dehydrates to a keto compound (**M3**).

Table 1. Molecular Weight, Mass of the Parent Ion, and Numbers of Retained Deuterium and ^{18}O Atoms for the Metabolites Obtained from the CYP125-Catalyzed Oxidation of Cholest-4-en-3-one

metabolite	peak	mol. mass (Da)	parent ion mass (m/z)	number of retained D atoms	number of retained ^{18}O atoms
Cholest-4-en-3-one	S	384.6	385.3 $[MH]^+$	7	n.a.
26-Hydroxycholest-4-en-3-one	III	400.6	401.3 $[MH]^+$	6	1
Cholest-4-en-3-one-26-aldehyde	II	398.6	399.3 $[MH]^+$	5	0
Cholest-4-en-3-one-26-acid	IV	414.6	415.3 $[MH]^+$	4	1 or 2[a]
27-Nor-cholest-4-en-3-one-26-ene (**M1**)	I	368.6	369.3 $[MH]^+$	3	0
27-Nor-25-oxyformyl-cholest-4-en-3-one (**M2**)	II	414.6	415.3 $[MH]^+$	5	1 or 2[a]
27-Nor-25-oxo-cholest-4-en-3-one (**M3**)	III	384.6	385.3 $[MH]^+$	3	1
27-Nor-25-hydroxy-cholest-4-en-3-one (**M4**)	V	386.6	387.3 $[MH]^+$	4	1
27-Nor-25,26-dihydroxy-cholest-4-en-3-one (**M5**)	VI	402.6	385.3 $[MH\text{-}H_2O]^+$	3	1

[a]Although two oxygen atoms are added, one can be exchanged with an oxygen of water, resulting in incorporation of only one labeled oxygen from $^{18}O_2$.

ing to stepwise oxidation of the side-chain to the cholest-4-en-3-one-26-acid.[17,19] Interestingly, we observed the formation of several additional products when the concentration of mβCD was decreased to 0.05% (w/v). Lowering the mβCD concentration decreases its competition for binding of the sterol metabolites. As shown in Figure 1, at least six peaks (**I**−**VI**) could be distinctly seen from a reverse-phase liquid chromatographic analysis of the reactions of CYP125 with cholest-4-en-3-one. Importantly, the fact that analysis of the oxidations of authentic 26-hydroxy-cholest-4-en-3-one and cholest-4-en-3-one-26-aldehyde by CYP125 yielded nearly identical elution profiles (Figure 1), but that of cholest-4-en-3-one-26-acid did not (data not shown), indicates that the unknown metabolites originated from competitive, concomitant reactions of the 26-aldehyde intermediate.

Mass Spectrometric Characterization of the Unknown Metabolites. We used LC−MS and 25,26,26,26,27,27,27-d_7-cholest-4-en-3-one to help determine the structures of the metabolites. We also carried out the reactions under an atmosphere of $^{18}O_2$ to help elucidate the mechanisms of their formation. Figure 2 displays the mass spectra of the three expected products as well as for one major (**M3**) and four minor (**M1**, **M2**, **M4** and **M5**) unidentified metabolites separated by liquid chromatography from the different incubations. The proposed structures of these metabolites are also presented. The masses of the parent and daughter ions of all the metabolites, which were confirmed by MS/MS, are summarized in Supporting Information Table S1. As expected, three of the products correspond to the previously characterized side chain oxidation metabolites, that is, 26-hydroxy-cholest-4-en-3-one (peak **III**, m/z 401 $[M + H]^+$), cholest-4-en-3-one-26-aldehyde (peak **II**, m/z 399 $[M + H]^+$), and cholest-4-en-3-one-26-acid (peak **IV**, m/z 415 $[M + H]^+$). The identities of these metabolites were previously confirmed using authentic standards. The identities of the new metabolites (**M1**−**M5**) were established as discussed below.

27-Nor-25-oxo-cholest-4-en-3-one (M3). Close inspection of the mass spectrum from peak **III** (Figure 1) revealed the presence of a second parent ion at m/z 385.3 (Figure 2). The mass difference (16 Da) argues that the species at m/z 385.3 is not a fragment ion of the 401.3 species. The mass difference of three when the heptadeuterated substrate is used, indicating only three deuterium atoms are retained, and of two when $^{18}O_2$ is used, indicating the incorporation of one oxygen atom (Figure 2), strongly suggest the metabolite is 27-nor-25-oxo-cholest-4-en-3-one.

The formation of **M3** can be rationalized by addition of the ferric−peroxo anion to the 26-aldehyde followed by homolytic

dx.doi.org/10.1021/ja211499q | J. Am. Chem. Soc. 2012, 134, 6673−6684

fragmentation to give Compound II and an alkoxy radical that secondarily fragments to a demethylated carbon radical. Recombination of the oxygen of Compound II with the carbon radical yields the 27-nor-25-hydroxy product (pathway b, Scheme 2). A second, conventional 25-hydroxylation of this compound by CYP125 then yields a *gem* diol that dehydrates to give the final 27-nor-25-keto metabolite. The intermediate 25-hydroxy compound is also detected (**M4**, see below). In accord with the data, this metabolite has lost four deuterium atoms and incorporates an atom of molecular oxygen (Table 1).

27-Nor-25-oxyformyl-cholest-4-en-3-one (M2). Close inspection of the mass spectrum of peak **II** revealed the presence of two parent ions at m/z 399.3 and 415.3 (Figure 2). The parent ion at m/z 399.3 corresponds to the 26-aldehyde with which **M2** co-elutes. Although the parent ion mass of m/z 415.3 is the same as that for the 26-acid, the large difference in the retention time (>2 min) precludes its identification as a 26-acid diastereomer. Moreover, the m/z value of the parent ion of the deuterated metabolite is 420.3, which is 5 Da rather than 4 Da higher, so that one of the three deuterium atoms of the methyl group that is oxidized is retained. This can be explained if the metabolite is a 27-nor-25-oxoformyl derivative, as shown. However, this metabolite has two oxygen atoms, but the $^{18}O_2$ data suggests that only one ^{18}O-atom is incorporated. This is not unexpected, as the 26-aldehyde from which the formyl is derived, like most aldehydes, can readily exchange its oxygen with water from the medium, resulting in loss of one of the two originally labeled oxygens.[36]

The formation **M2** could occur via the trapping of a C25 carbocation by the formate ion generated in the deformylation step. In turn, the carbocation could be generated by single-electron oxidation of the C25 radical generated by homolytic decomposition of a peroxyhemiacetal intermediate (pathway c, Scheme 2). Alternatively, the formation of **M2** could result from a rearrangement of the peroxyhemiacetal adduct via an ionic Baeyer−Villiger mechanism, similar to that proposed for CYP51-mediated lanosterol demethylation (not shown).[37]

27-Nor-25-en-cholest-4-en-3-one (M1). A single metabolite **M1** with an m/z of 369.3 was detected in peak **I** (Figure 1). Its low polarity, its retention of three deuterium atoms in the reaction with the heptadeuterated sterol substrate, and the absence of a mass increase in the presence of $^{18}O_2$ suggest that it is the 27-nor-25-ene derivative (Figure 2). Furthermore, the presence of three atoms of deuterium in the deuterated product (m/z 372.3) argues against formation of the isomeric 27-nor-cholest-4-en-3-one-24-ene, a metabolite containing an internal double bond between the C24 and C25 positions, as it would retain four, and not three, deuterium atoms.

The formation of this product is readily rationalized by the same manifold used to explain the formation of **M2** and **M3**. Homolytic fragmentation of the peroxyhemiacetal generated by addition of the ferric−peroxo anion to the 26-aldehyde generates a carbon radical that, by transfer of one electron to the enzyme, is converted to a C25-cation (pathway c, Scheme 2). Loss of a proton (or deuterium) then produces the terminal olefin (pathway d, Scheme 2). Alternatively, abstraction of a terminal proton from the C25 radical intermediate by Cpd II could also result in the direct formation of **M1** (pathway a, Scheme 2).

Alternate mechanisms for the formation of an alkene involving a Cpd I intermediate were considered for human aromatase CYP19.[29,38] One such mechanism involves hydroxylation two atoms away from the aldehyde carbon, but this mechanism would require introduction of a double bond in our sterol molecule between C24 and C25, which is not observed. Alternatively, the hydroxylation could take place at the other methyl group of the side chain, but only one of the products, the terminal olefin M1, can be accommodated by this mechanism. Furthermore, this mechanism is unlikely as it involves an energetically unfavorable four-membered ring in the transition state. Another mechanism that has been proposed involves formation of the gem diol from the aldehyde (or from the alcohol) followed by oxidation of this species by Cpd I-mediated hydrogen abstraction, one electron oxidation, and C−C bond cleavage to produce the alkene.[38] However, the support for this mechanism drawn from gas phase computational studies has been negated by more recent studies by the same group with a more sophisticated computational model.[39] Another Cpd I mediated mechanism that involves initial hydroxylation 3 carbons away from the aldehyde carbon to form an alkene[29] is untenable as it fails to generate the desired product.

27-Nor-25-hydroxy-cholest-4-en-3-one (M4). A metabolite eluted in low abundance was detected in peak **V**. The MS (Figure 2) and MS/MS (Table S1) of this metabolite revealed, respectively, a parent ion $[M + H]^+$ at m/z 387 and a daughter ion $[(M + H) - H_2O]^+$ at m/z 369, in accord with a structure containing an alcohol group. The lower mass and the shorter retention time, compared to 26-hydroxy-cholest-4-en-3-one (peak **IV**) suggest that the substrate underwent oxidative loss of one of the two terminal methyl groups with incorporation of a hydroxyl group at C25. We thus propose that this metabolite is 27-nor-25-hydroxy-cholest-4-en-3-one. This structure is confirmed by the retention of 4 deuterium atoms from the heptadeuterated cholest-4-en-3-one substrate and by the incorporation of one atom of $^{18}O_2$ (+2 Da) (Table 1). Interestingly, the MS analysis of the reaction performed in the presence of $^{18}O_2$ revealed the additional presence of this metabolite without incorporation of the heavier oxygen isotope (Figure 2). This observation could be explained by contamination of the $^{18}O_2$ with $^{16}O_2$, but this is unlikely as this contamination was not observed with any of the other oxygenated metabolites.

The formation of **M4** is most consistent with radical decomposition of a peroxyhemiacetal adduct to form the C25 radical species that then recombines with the Compound II ferryl oxygen (pathway b, Scheme 2). The detection of $^{16}O_2$-containing **M4** metabolite when the reaction was performed under an atmosphere of $^{18}O_2$ is readily explained by oxidation of the C25 radical to the cation, as already postulated above for formation of the formyl adduct, followed by trapping by a water molecule rather than formate ion (pathway e, Scheme 2).

27-Nor-25,26-dihydroxy-cholest-4-en-3-one (M5). Finally, in peak **VI**, we detected a major species with m/z value of 385 (Figure 2). This product retained three deuterium atoms of the original seven in heptadeutero cholest-4-en-3-one and, from the shift of 2 units with $^{18}O_2$, incorporated one atom of molecular oxygen (Table 1). We propose that this metabolite is 27-nor-25,26-dihydroxy-cholest-4-en-3-one for which the major ion, as observed, corresponds to the loss of a water molecule $[(M + H) - H_2O]^+$. This compound would result from CYP125-catalyzed epoxidation of **M1** followed by acid catalyzed epoxide hydrolysis, which would introduce the second oxygen from water rather than oxygen gas. In principle, it could arise from hydroxylation of **M4**, but that would introduce two atoms of molecular oxygen. Finally, CYP125-

catalyzed oxidation of a synthetic, authentic sample of 27-nor-25-en-cholesterol confirmed the epoxidation of the terminal alkene and its subsequent acid-catalyzed ring opening to yield a vicinal diol with a retention time similar to that of **M5**.

Expression, Purification, and UV–Vis Spectrophotometric Characterization of SeCYP125. As CYP125 possesses three cysteines, we prepared the C172S/C429L mutant to remove the two cysteines other than the one coordinated to the heme iron atom. The selenium substituted CYP125, SeCYP125, was expressed and purified from this construct using minimal media in the presence of selenocysteine, as described elsewhere.[34] About 3–4 mg/L of the SeCYP125 was obtained after affinity purification, which is ~4 fold less than the yield of the WT* protein expressed using the media containing cysteine. Our selenocysteine incorporation approach resulted in introduction of a selenocysteine only at the iron coordinating position.

SeCYP125 exists as a mixture of ferric high spin (HS) and low spin (LS) complexes with absorption maxima at 393 and 417 nm, respectively, along with broader peaks at 532 and 570 nm corresponding to the α and β bands, and a CT band at 643 nm. This contrasts with the WT* protein, which is predominantly in the high spin form with a large peak at 395 nm bearing only a small shoulder at 416 nm (Figure 3A). On the basis of the UV–vis spectrum, SeCYP125 appears to contain about 40% of the heme in the low-spin form.

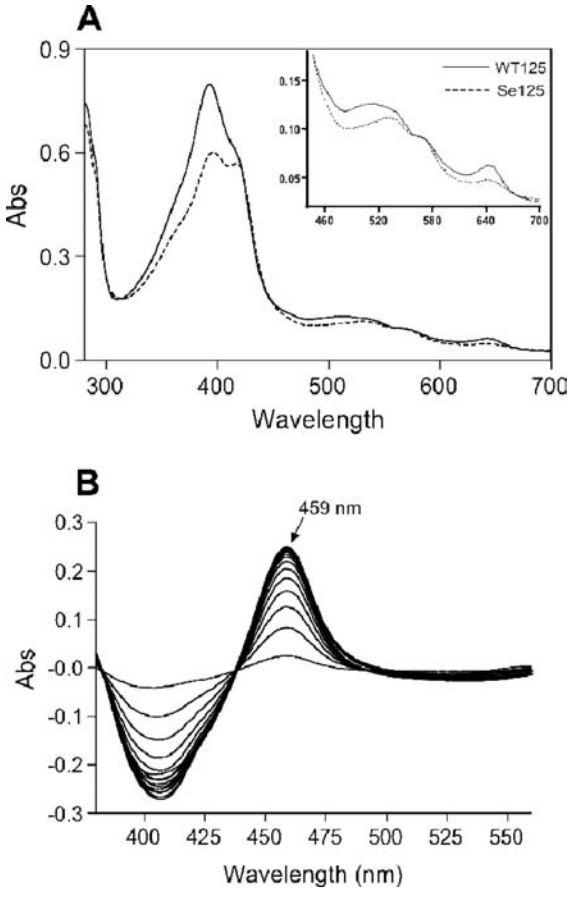

Figure 3. UV–vis spectrophotometric characterization of SeCYP125. (A) Comparison of the native ferric spectrum of the WT* and SeCYP125 proteins in 100 mM potassium phosphate buffer, pH 7.4. (B) Fe^{2+}–CO difference spectrum of the SeCYP125 measured over 12 min, at 1 min intervals, after the addition of 1 mM dithionite.

Replacement of the cysteine by selenocysteine clearly leads to tighter binding of the distal water molecule coordinated to the heme iron atom and an increased stability of the low-spin form. The Fe(II)–CO complex of SeCYP125 with a Soret band at 459 nm (Figure 3B) exhibits a 9 nm red shift relative to that of the WT* protein at 450 nm. As reported earlier for selenium substituted CYP119 and CYP101,[40,41] this red shift of the Fe(II)–CO spectrum is consistent with introduction of the electron rich selenolate as the proximal ligand.

Characterization of SeCYP125 by Resonance Raman and EPR Spectroscopy. The resonance Raman (RR) spectra of the ferric forms of WT* and SeCYP125 clearly indicate that selenium substitution has stabilized the distal water bound low spin species, in agreement with what was observed in the UV–vis spectra. The RR spectrum of WT* CYP125 shows ν_4, ν_3, and ν_2 at 1373, 1488, and 1574 cm^{-1}, respectively, and confirms the predominance of the HS species over LS species identified by ν_3 and ν_2 at 1502 and 1584 cm^{-1} (Figure 4). In contrast, the

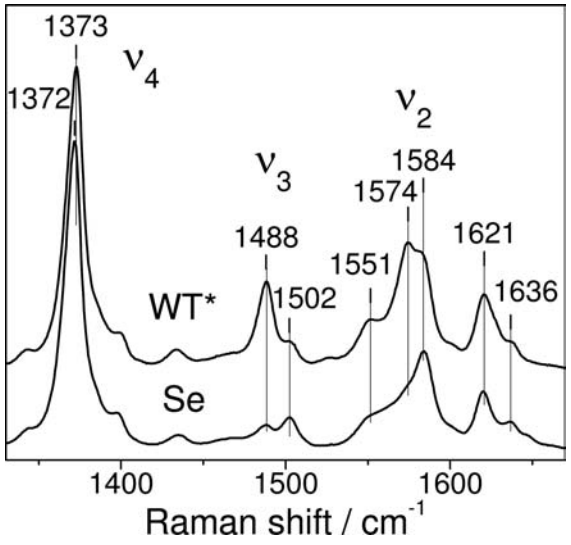

Figure 4. Resonance Raman spectra of Fe^{3+} WT* and SeCYP125. Room temperature RR spectra obtained with a 413 nm excitation.

LS marker bands are dominant contributions in the RR spectrum of SeCYP125 compared to the WT* protein. Substituting the heme iron axial sulfur with selenium in SeCYP125 downshifts the ν_4 mode 1 cm^{-1} which may reflect an increased electron density on the antibonding porphyrin π^* orbitals, as previously observed with SeCYP119.[40] The ν_4 downshift in SeCYP125 is smaller than the 2-cm^{-1} downshift observed in SeCYP119, but it may be due to the weak dependence of this mode on the Fe^{3+} spin state.

The similarity of the impact of the sulfur to selenium substitution in SeCYP125 and SeCYP119 is also evident from the EPR spectra of the ferric low-spin species.[40] The EPR spectrum of WT* shows g values at 2.4, 2.25 and 1.94, as previously reported.[18] New resonances with increased g values at 2.45, 2.29, and 1.98 dominate the EPR spectrum of SeCYP125 (Figure 5). Minor contributions corresponding to the WT* resonances indicate that the cysteine substituted protein is present as a contaminant; While these minor signals vary in intensity between different preparations, they consistently remain below 20% of the total low spin signal.

The Fe^{3+}–NO complexes of WT* and SeCYP125 were also characterized by RR spectroscopy with 442-nm Soret

dx.doi.org/10.1021/ja211499q | J. Am. Chem. Soc. 2012, 134, 6673–6684

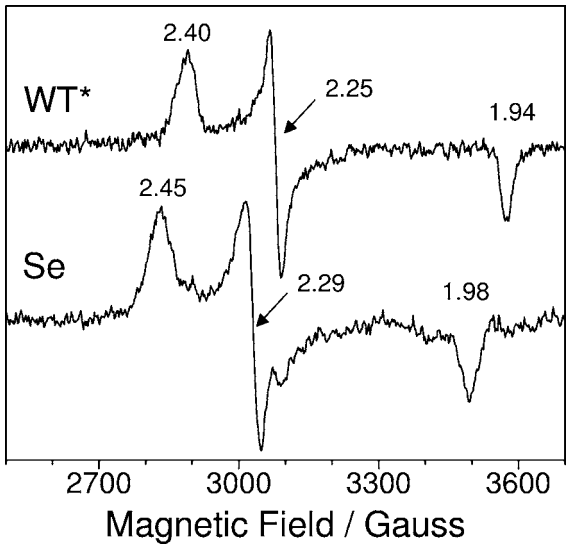

Figure 5. EPR spectra of Fe^{3+} WT* and SeCYP125. EPR spectra of Fe^{3+} WT* and SeCYP125 at 10 K. Microwave frequency, 9.66 GHz; microwave power, 0.01 mW; modulation amplitude, 10 G.

excitation. In the low-frequency RR spectra of WT*, intense vibrations at 521 and 549 cm^{-1} downshift with ^{15}NO and are assigned to mixtures of bending and stretching modes, that is, ν(Fe−NO) and δ(Fe−N−O), respectively (Figure 6). While substrate-free P450 heme Fe^{3+}−NO complexes typically exhibit a single band assigned to the ν(Fe−NO), substrate binding promotes the enhancement and mixing of δ(Fe−N−O) mode as the Fe−N−O unit deviates from linearity; this trend has been particularly well documented in P450cam by Hu and Kincaid.[42] Presumably, distal pocket residues in CYP125 promote a bent Fe−N−O geometry even in the absence of substrate. While the low-frequency RR spectra of the Fe^{3+}−NO complex in SeCYP125 are remarkably similar to those of WT*, the sulfur to selenium substitution downshifts the ν(Fe−NO) and δ(Fe−N−O) vibrations from 521 to 519 cm^{-1} and from 549 to 541 cm^{-1} (Figure 6). These modest downshifts are comparable to those observed earlier with the nitrosyl complex of SeCYP119.[40] In the high-frequency region of the RR spectrum of WT*, the ν(N−O) mode is identified at 1835 cm^{-1} as its 34-cm^{-1} ^{15}N-downshift matches the calculated value based on an isolated diatomic oscillator. The sulfur to selenium substitution downshifts the ν(N−O) mode to 1819 cm^{-1}; an equivalent downshift of the ν(N−O) mode was observed in CYP119 upon substitution of the trans ligand.[40] In addition to the ν(N−O) modes, a second isotope sensitive signal is observed above 1900 cm^{-1} in WT* and SeCYP125, but the small ^{15}N-isotope shifts these bands exhibits identified them as combination mode between ν(Fe−NO)/δ(Fe−N−O) and the ν_4 mode which occur at 1375 cm^{-1} in the ferric−nitrosyl complexes. The concomitant decreases of all vibrations involving the NO upon substitution of the sulfur ligand with selenium can be interpreted in terms of competing σ-trans effect between the two axial ligands. As with our earlier study of SeCYP119, the RR results support the notion that the sulfur to selenium substitution increased electron donation from the proximal ligand to the heme iron.

SeCYP125 Binds and Catalyzes the Oxidation of Cholest-4-en-3-one. The binding and catalytic activities of SeCYP125 were tested using cholest-4-en-3-one as a substrate. The binding of a substrate-like molecule to P450 enzymes

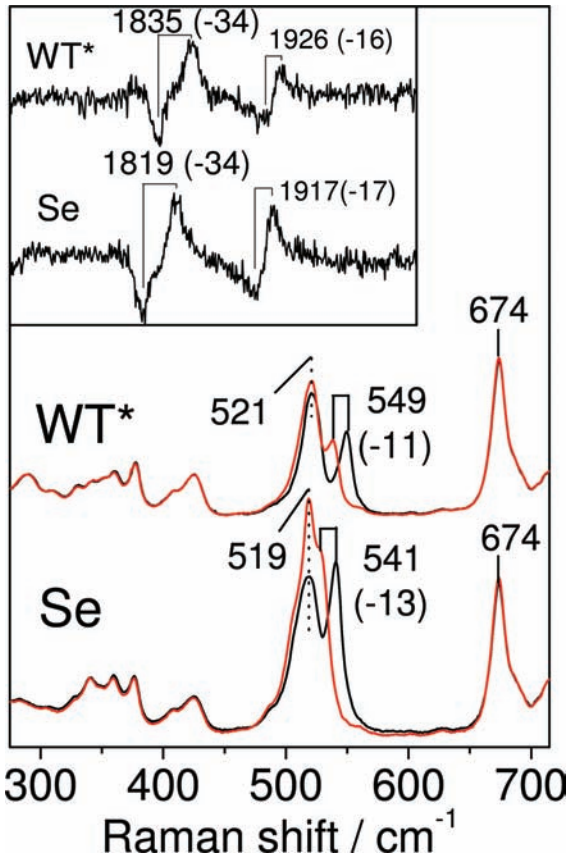

Figure 6. Resonance Raman spectra of Fe^{3+}−NO complexes. Room temperature RR spectra of the Fe^{3+}−NO complexes of WT* and SeCYP125 prepared with ^{14}NO and ^{15}NO. All spectra were obtained with a 442 nm excitation. The low-frequency spectra were normalized on the ν_7 at 674 cm^{-1}. The inset shows ^{14}NO minus ^{15}NO high-frequency difference spectra obtained after normalization on the ν_4 mode at 1375 cm^{-1}.

typically results in displacement of the water molecule coordinated to the heme iron and consequently in a spectroscopically detectable low-spin to high-spin transition known as a type-I shift. The K_D values of WT* and SeCYP125 for cholest-4-en-3-one calculated from titration curves (Figure 7A) are 0.71 ± 0.05 and 2.28 ± 0.11 μM, respectively. A 3-fold decrease in the binding affinity for SeCYP125 is consistent with the greater stability of the water-bound low-spin state.

The enzymatic activity of SeCYP125 was analyzed in vitro and was compared to that of the WT* enzyme. As shown in Figure 7B, SeCYP125 also efficiently catalyzes the oxidation of cholest-4-en-3-one, as judged by the appearance of six peaks in the HPLC chromatogram. The activity of SeCYP125 toward cholest-4-en-3-one is very similar to that of the WT* with 82% of the substrate consumed after 60 min, compared to 86% for WT*. MS analysis also confirmed that the metabolites produced by SeCYP125 were identical to those generated by the WT* enzyme (not shown). These findings clearly indicate that replacement of the cysteine by a selenocysteine has not altered the nature of the active site, as the substrate binding and the net reactivity of the SeCYP125 remain highly comparable to those of the WT* protein.

Kinetic studies show that the k_{cat} for formation of 26-hydroxy cholest-4-en-3-one, calculated as 49 min^{-1} for the WT* enzyme, is approximately 2-fold faster than the rate observed for SeCYP125 (Table S3, Supporting Information). In contrast,

dx.doi.org/10.1021/ja211499q | J. Am. Chem. Soc. 2012, 134, 6673−6684

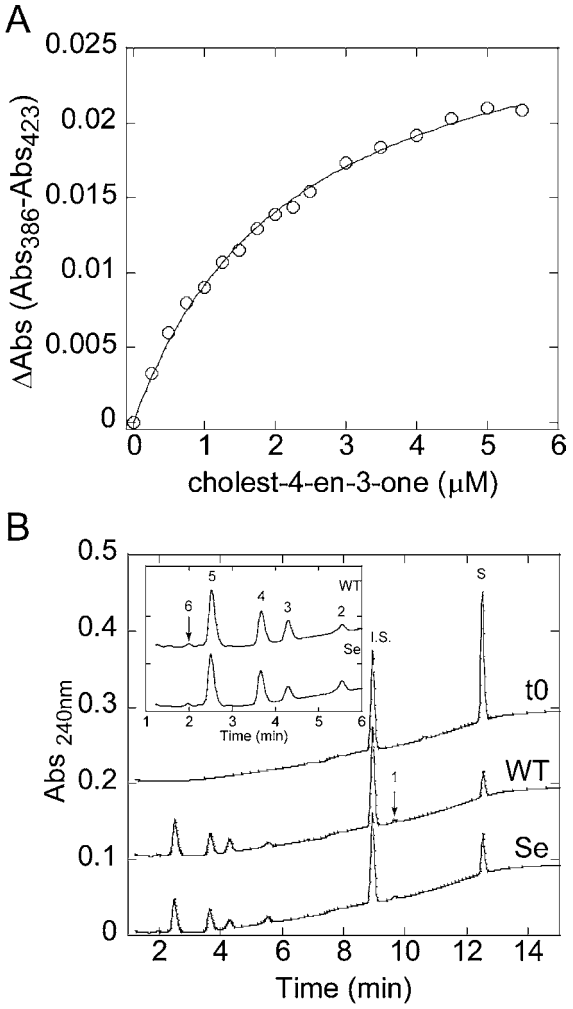

Figure 7. Binding and catalytic activities of SeCYP125 toward cholest-4-en-3-one. (A) Binding of cholest-4-en-3-one to recombinant SeCYP125. The concentration dependence of ligand binding was deduced from the difference in absorption changes obtained from titration of the protein (2.5 μM P450) with increasing concentrations of cholest-4-en-3-one. The data was fit using a tight binding equation.[19] (B) LC chromatograms with absorbance detection at 240 nm of the WT* and SeCYP125 oxidation products of cholest-4-en-3-one, separated using a reverse phase C-18 Xterra column (Waters), as described in the Experimental Procedures. A control reaction carried out in the absence of NADPH is also included. Inset: zoom-in showing the HPLC elution of the minor products. S and I.S. stand for substrate and internal standard, respectively.

the steady-state rate constant measured for the second oxidation from the 26-hydroxy to 26-aldehyde was approximately 3-fold faster for SeCYP125 than for the WT*. Although the rates are comparable between the WT* and SeCYP125 for each step, they are significantly different for the individual enzymes. In contrast, the K_m values for binding of the two substrates to the WT and SeCYP125 enzymes are very similar.

Product Distributions in the Turnover of Cholesterol-26-aldehyde by WT* and SeCYP125. WT* and SeCYP125 clearly produce a 26-aldehyde intermediate that can undergo monooxygenation to generate the corresponding 26-acid. As shown here, the aldehyde is also oxidized via a peroxyhemiacetal intermediate to the C−C bond cleavage products **M1**−**M5**, providing an opportunity to investigate the influence of increased electron donation from the proximal iron ligand on the monooxygenation versus deformylation pathways. For this purpose, we compared the oxidation of the cholesterol 26-aldehyde itself by the WT* and SeCYP125 proteins. Focusing on the oxidation of the cholesterol 26-aldehyde is desirable because the aldehyde sits at the branching point between the two pathways. The metabolites were quantitated as the ratio of the total mass spectrometric ion current of the individual metabolites to the signal from the known amount of internal standard (Experimental Procedures). The effect of increased electron donation was then determined by comparing the amount of the 26-acid produced to the sum of the products originating from the deformylation pathway for the WT* and SeCYP125-mediated oxidations.

The oxidation of the cholesterol-26-aldehyde by the WT* and SeCYP125 proteins generated similar products (Figure S1, Supporting Information). The oxidation reaction was very efficient as more than 90% of the substrate was oxidized by both enzymes. More importantly, the oxidation of the 26-aldehyde by SeCYP125 produced a significantly higher amount of the 26-acid and lesser amounts of the deformylation products, with 27-nor-25-oxo-cholesterol formed as the major deformylation product. Overall, the ratio of the 26-acid to the sum of the deformylated products was found to be ~1.3-fold higher with SeCYP125 than with the WT* protein (Figure 8). It should be stressed that not only was the difference in the ratio between the two enzymes highly reproducible, but virtually identical differences in the ratio were observed when either 26-hydroxycholesterol or cholesterol was used as the substrate (Figure 8).

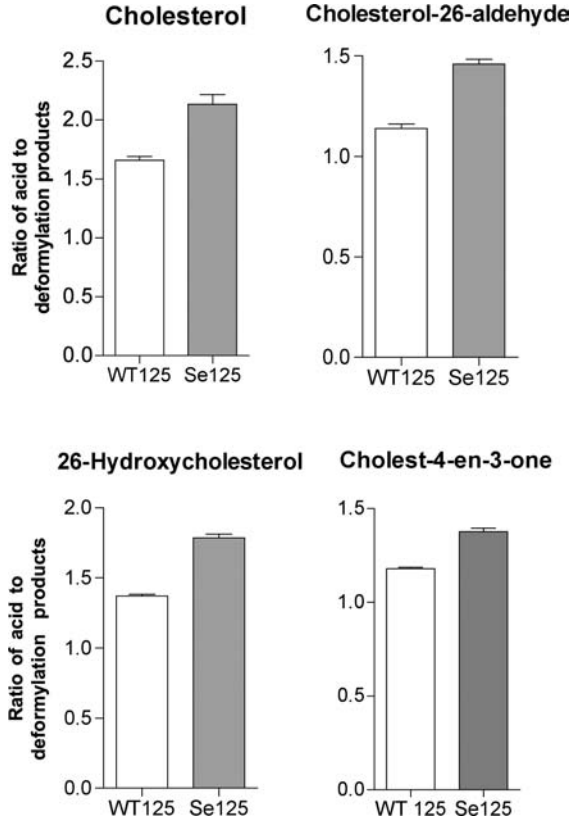

Figure 8. Comparison of the ratio of the 26-acid over the sum of the deformylation products produced during the oxidation of various substrates by WT* and SeCYP125 after 60 min incubation.

dx.doi.org/10.1021/ja211499q | J. Am. Chem. Soc. 2012, 134, 6673−6684

In contrast, although the ratios between WT and SeCYP125 were identical for cholesterol and its 26-alcohol and 26-aldehyde products, a smaller increase of ~1.2-fold was observed when cholest-4-en-3-one was used as the substrate. Furthermore, the ratios of the acid to deformylation products were not identical for the same enzyme when compared for different substrates. Thus, ratios of 1.6, 1.4, and 1.2 were observed for the WT* enzyme with the cholesterol, 26-hydroxy and 26-aldehyde substrates, respectively (Figure 8).

DISCUSSION

As shown here, oxidation of the cholesterol side-chain by CYP125 leads to the formation not only of the C26-acid, as previously reported,[19] but also of five additional products (**M1**−**M5**) resulting from C−C bond cleavage. The formation of these additional products was uncovered by varying the incubation conditions and carefully analyzing the product HPLC peaks. The identities of the metabolites were established by comparison with authentic standards or by mass spectrometry in combination with deuterium labeling and the use of $^{18}O_2$ in the oxidation reaction. The mechanisms proposed for formation of the C−C bond cleavage products (Scheme 2) are fully consistent with the deuterium and oxygen labeling results and with the general mechanisms proposed for such reactions.[29−31,43] None of the reactions leading to the observed products were entirely unprecedented, but the co-occurrence of this diversity of products in the catalytic turnover of a single substrate by a P450 enzyme is highly unusual. This product diversity has provided us with a tool with which to examine the effect of electron donation from the proximal ligand on formation of the Compound I species.

The role of Compound I in monooxygenation reactions is well documented. Similarly, growing evidence points to the ferric−peroxo anion intermediate as the active oxidant in C−C bond cleavage reactions. All this evidence clearly supports the role of the ferric−peroxo anion in the generation of deformylation products. Thus, the feasibility of the reaction is established by nonenzymatic deformylation of the 19-aldehyde of androstenedione by a porphyrin ferric−peroxo anion model complex.[44] Trapping of the ferric−peroxo anion in CYP19 using cryo-freeze quench EPR methods confirms the biological existence of this intermediate and bolsters its potential role in deformylation reactions.[45] More directly, the use of radio-labeled substrates and $^{18}O_2$ has clearly established the involvement of the ferri−peroxo anion in the formation of acyl-carbon bond cleavage products by CYP51[31] and CYP17,[43] results that specifically rule out the participation of a Compound I intermediate. Furthermore, consistent with nucleophilic attack of the peroxo anion on the aldehyde, a distal H-bonding mutant in CYP2B4 that blocks the protonation of the peroxy anion, generated more deformylated metabolites relative to the Compound I-mediated monooxygenation product.[46] The peroxy anion mechanism was recently supported by a detailed theoretical analysis.[39] Finally, in the present case, the total number of deuterium atoms retained by the metabolites after the oxidation of cholesterol with the heptadeuterated side chain, excludes alternative mechanisms involving a Compound I intermediate. The branchpoint intermediate in generating the acid and all the C−C bond cleavage products is the C26 aldehyde (Scheme 1). On the basis of literature precedent, it is likely that the 26-aldehyde acts as the common precursor of all the end products since the same products, and similar product distributions, are obtained when the aldehyde is provided as a substrate (Table S2) as when the aldehyde is generated internally from cholesterol or 26-hydroxy cholesterol through initial oxidative turnovers. In this system, the formation of products from the Compound I-mediated monooxygenation and peroxyhemiacetal-mediated deformylation pathways is controlled by the intrinsic reactivity of the ferric−peroxo anion intermediate. To investigate the effect of increased electron donation from the proximal ligand on partitioning of the aldehyde intermediate into the two reaction pathways, we expressed CYP125 with a selenocysteine replacing the cysteine that provides the proximal thiolate iron ligand.

The introduction of selenocysteine (SeCys) as the proximal iron ligand in a cytochrome P450 enzyme has recently been reported.[40,41] Unlike other proximal ligand substitutions, the SeCys proteins retain spectroscopic and catalytic properties comparable to those of their cysteine counterparts, although increased electron donation by the selenolate versus thiolate ligand does cause some differences. These include a shift to longer wavelengths of the Soret maxima of the Fe^{2+}−CO complexes and a lowering of the redox potentials of the enzymes.[34,41] In agreement with these earlier findings, the Soret maximum of the SeCys-substituted CYP125 utilized in these studies was at 459 nm rather than the 450 nm found for the WT* protein. The position of this Soret indicated a high degree of incorporation of SeCys into the protein, an inference supported by the near absence of EPR resonances from the WT* enzyme in the EPR spectrum of SeCYP125 (Figure 5). Furthermore, comparison of the resonance Raman spectra of the ferric and ferric-nitrosyl hemes in WT* and SeCYP125 proteins show that the SeCys substitution increases electron donation to the metal iron.

More importantly, SeCYP125 binds cholest-4-en-3-one with a similar affinity to that of the WT* enzyme and oxidizes this substrate to the same products, albeit not in exactly the same ratios. When the reaction is run with cholesterol 26-aldehyde as the substrate, both enzymes consume the substrate to essentially the same degree after 60 min, so the differences in product ratios are not due to differential extents of substrate utilization. This result also argues that factors such as differential uncoupling of the two enzymes is not a factor in determining the differences in the product ratios, as higher uncoupling would lead to slower consumption of the aldehyde. It should also be emphasized that the ratio of the products starting with the aldehyde is the most relevant to the conclusions of this paper, as it directly compares the reactions at the branchpoint without any confounding factors that might arise from a requirement for multiple turnovers prior to generating the aldehyde. With both enzymes, all the C−C bond cleavage products are formed, but the 26-acid metabolite is the major product. The primary finding is that the SeCYP125-mediated oxidation produces more cholesterol 26-acid relative to the sum of the C−C bond cleavage products than the WT*. The 1.3-fold increase in the ratio of the 26-acid to deformylation products indicates that selenocysteine substitution favors the formation of Compound I. The oxidation of cholesterol and 26-hydroxycholesterol, the two precursors of the aldehyde, by SeCYP125 also yielded an ~1.3-fold increase, relative to the WT*, in the ratio of the acid to homolysis products (Figure 8). Finally, oxidation of 25,26,26,26,27,27,27-d_7-cholesterol by the WT* enzyme was examined. The results show that even with deuterated cholesterol, the amount of acid produced is enhanced relative to the sum of deformylation

dx.doi.org/10.1021/ja211499q | J. Am. Chem. Soc. 2012, 134, 6673−6684

products. This result argues against any mechanism in which both carboxylic acid formation and decarboxylation are mediated by the ferryl species.

Although the differences in the product ratios obtained with the WT* and SeCYP125 enzymes are essentially identical among the cholesterol derivatives, the product ratios for the same enzyme varied significantly for the different substrates. The steady-state amounts of the cholesterol 26-aldehyde remaining at the end of the 60 min incubation of WT* enzyme with cholesterol and 26-hydroxy cholesterol were calculated to be ∼5 and 2.8 μM, respectively. Similarly for SeCYP125, the amounts of cholesterol 26-aldehyde remaining were ∼5.8 and 3.1 μM. Although more aldehyde reacted when 26-hydroxy cholesterol was the substrate, overall the amounts of aldehyde reacted with WT* and SeCYP125 at the 60 min time point were comparable.

The ratio of the products differed when the substrate was changed from cholesterol or its 26-oxidized products to cholest-4-en-3-one. This finding is not surprising, as there is no reason to expect that the 3-keto-26-aldehyde generated from cholest-4-en-3-one will bind in the active site and will interact with the protein residues in exactly the same manner as the 3-hydroxy-26-aldehyde of cholesterol. Nevertheless, it is clear that with this substrate the carboxyl-forming branch of the reaction is also favored by selenolate ligation to the iron. More surprising is the finding that the ratio of products exhibited some variation for a given enzyme when comparing the degradation of cholesterol, 26-hydroxycholesterol, and the cholesterol 26-aldehyde. A constant ratio would be expected if no factors intervened other than the intrinsic partitioning of the product pathways at the aldehyde stage. There is no evidence for allosteric effects of cholesterol or its oxidation products on CYP125 catalysis. It is possible that this variation results from a channeling effect that occurs when the substrate is cholesterol or 26-hydroxycholesterol. As shown by the UV−vis binding experiments, a water molecule is displaced from the heme iron on binding of the substrate. This water molecule may slightly perturb the hydrogen bonding pattern in the active site during catalytic turnover, but more importantly, this perturbation may not be the same when a substrate such as cholesterol binds to the enzyme two catalytic turnovers prior to the one that controls the product ratio. Of course, this argument only applies if, at least to some extent, the substrate is processed through multiple turnovers without dissociating from the protein. Interestingly, channeling in the oxidation of aldehydes generated in situ from precursor molecules has been reported in the reactions of CYP2A6.[47]

Partitioning of the ferric−peroxo anion intermediate between conversion to Compound I (leading to acid formation) and addition to the aldehyde to give a peroxyhemiacetal (leading to C−C bond cleavage) hinges on the extent to which the intermediate is present as the peroxy anion versus the hydroperoxide. Increased electron donation from the proximal thiolate to the iron bound dioxygen is proposed to increase the pK_a of Compound 0.[27] Computational studies suggest that the more electron-donating selenolate proximal ligand should enhance the rate of formation of Compound I.[48] In our studies, an increase in the pK_a of the peroxy anion would result in a shift from the anionic toward the hydroperoxo form, and this shift would result in increased formation of Compound I and decreased formation of the peroxyhemiacetal intermediate. This predicts an increased oxidation of the aldehyde to the carboxylic acid at the expense of the deformylation products, as observed here. To our knowledge, this is the first direct evidence emphasizing the role of increased electron donation from the proximal ligand leading to enhanced electron density on the distal oxygen of the ferric-peroxo anion intermediate.

Protonation of the ferric−peroxo anion depends, of course, on the availability of a suitable proton donor on the distal side of the heme. Thus, a number of studies have shown that replacement of a highly conserved distal threonine thought to be involved in this process leads to decreased catalysis and increased uncoupling.[46,49] However, in the present instance, the distal Thr272 and its environment are unchanged and cannot be the cause of the difference in protonation of the ferric−peroxo anion.

The change of 1.2- to 1.3-fold in the ratio of the acid to deformylation products is significant but modest. Importantly, identical ratios are reproducibly observed with both cholesterol and cholest-4-en-3-one, as well as when the 26-alcohol and 26-aldehyde derivatives are used instead of the parent steroids as the substrates. It is difficult to predict the change in the pK_a value of the distal oxygen of the ferric−peroxo anion intermediate when a selenolate replaces the thiolate ligand, but the change is not likely to be large. Thus, the expected changes in product ratios should be modest, as observed. Moreover, as the increased electron density on the peroxy anion increases its nucleophilic character, it may promote its addition to the aldehyde and lower the acid to deformylation product ratios.

The extensive partitioning between monooxygenation and deformylation of the C26 aldehyde seen in the oxidation of cholesterol by CYP125 is unique among the known steroid C26-monooxygenases, as CYP27A1, CYP124, and CYP142 produce the alcohol, aldehyde, and acid metabolites without detectably forming the deformylation products.[16,17,19,32,50] Thus, the ferric−peroxo anion intermediate in these latter enzymes is either protonated much more quickly than in CYP125, or its possible addition to the aldehyde carbonyl group is suppressed within the active site.

■ CONCLUSION

In conclusion, we demonstrate the unique ability of CYP125A1 to catalyze the oxidation of the cholesterol side chain not only to the acid, but also to five other metabolites stemming from the deformylation of the intermediate aldehyde. Furthermore, a proximal selenocysteine substituted CYP125 enzyme was expressed, purified, and characterized using various spectroscopic methods. This enzyme was utilized to probe the effect of excess electron donation by the proximal ligand on the partitioning of the products between heterolytic (Compound I) and homolytic (deformylation) pathways. These experiments reveal that the increased electron donation from the proximal ligand to the iron favors protonation of the ferric−peroxo anion intermediate to form Compound I.

■ ASSOCIATED CONTENT

Supporting Information

Tables with LC−MS and MS/MS data, kinetic constants for the reactions, LC spectrum of the 26-aldehyde derivative, and a representative kinetic plot are available. This material is available free of charge via the Internet at http://pubs.acs.org.

dx.doi.org/10.1021/ja211499q | J. Am. Chem. Soc. 2012, 134, 6673−6684

AUTHOR INFORMATION

Corresponding Author

ortiz@cgl.ucsf.edu

Present Address

‡Department of Biological Sciences and The Border Biomedical Research Center, University of Texas, 500 W. University, El Paso, Texas 79968

Notes

The authors declare no competing financial interest.

ACKNOWLEDGMENTS

We thank Arti Singh and Prof. James De Voss of the University of Queensland for kindly providing us with the synthetic standard of 27-nor-25-en-cholesterol and Dr. Jonathan Johnston for helpful discussions and suggestions. This research was supported by National Institutes of Health Grants GM25515 and AI074824 (to P.R.O.M.) and GM74785 (P.M.-L.), and by National Center for Research Resources Grants P41RR001614 and RR019934 [to the Bio-Organic Biomedical Mass Spectrometry Resource at the University of California (director, A. L. Burlingame)].

REFERENCES

(1) Nelson, D. R. *Hum. Genomics* **2009**, *4*, 59.
(2) Rendic, S. *Drug Metab. Rev.* **2002**, *34*, 83.
(3) Andersen, J. F.; Tatsuta, K.; Gunji, H.; Ishiyama, T.; Hutchinson, C. R. *Biochemistry* **1993**, *32*, 1905.
(4) Cryle, M. J.; Meinhart, A.; Schlichting, I. *J. Biol. Chem.* **2010**, *285*, 24562.
(5) Cupp-Vickery, J. R.; Han, O.; Hutchinson, C. R.; Poulos, T. L. *Nat. Struct. Biol.* **1996**, *3*, 632.
(6) Julien, B.; Shah, S. *Antimicrob. Agents Chemother.* **2002**, *46*, 2772.
(7) Kells, P. M.; Ouellet, H.; Santos-Aberturas, J.; Aparicio, J. F.; Podust, L. M. *Chem. Biol.* **2010**, *17*, 841.
(8) Mendes, M. V.; Anton, N.; Martin, J. F.; Aparicio, J. F. *Biochem. J.* **2005**, *386*, 57.
(9) Ogura, H.; Nishida, C. R.; Hoch, U. R.; Perera, R.; Dawson, J. H.; Ortiz de Montellano, P. R. *Biochemistry* **2004**, *43*, 14712.
(10) Sherman, D. H.; Li, S.; Yermalitskaya, L. V.; Kim, Y.; Smith, J. A.; Waterman, M. R.; Podust, L. M. *J. Biol. Chem.* **2006**, *281*, 26289.
(11) Xue, Y.; Zhao, L.; Liu, H. W.; Sherman, D. H. *Proc. Natl. Acad. Sci. U.S.A.* **1998**, *95*, 12111.
(12) Zerbe, K.; Pylypenko, O.; Vitali, F.; Zhang, W.; Rouset, S.; Heck, M.; Vrijbloed, J. W.; Bischoff, D.; Bister, B.; Sussmuth, R. D.; Pelzer, S.; Wohlleben, W.; Robinson, J. A.; Schlichting, I. *J. Biol. Chem.* **2002**, *277*, 47476.
(13) Hawkes, D. B.; Adams, G. W.; Burlingame, A. L.; Ortiz de Montellano, P. R.; De Voss, J. J. *J. Biol. Chem.* **2002**, *277*, 27725.
(14) Capyk, J. K.; Kalscheuer, R.; Stewart, G. R.; Liu, J.; Kwon, H.; Zhao, R.; Okamoto, S.; Jacobs, W. R., Jr.; Eltis, L. D.; Mohn, W. W. *J. Biol. Chem.* **2009**, *284*, 35534.
(15) Rosloniec, K. Z.; Wilbrink, M. H.; Capyk, J. K.; Mohn, W. W.; Ostendorf, M.; van der Geize, R.; Dijkhuizen, L.; Eltis, L. D. *Mol. Microbiol.* **2009**, *74*, 1031.
(16) Driscoll, M. D.; McLean, K. J.; Levy, C.; Mast, N.; Pikuleva, I. A.; Lafite, P.; Rigby, S. E.; Leys, D.; Munro, A. W. *J. Biol. Chem.* **2010**, *285*, 38270.
(17) Johnston, J. B.; Ouellet, H.; Ortiz de Montellano, P. R. *J. Biol. Chem.* **2010**, *285*, 36352.
(18) McLean, K. J.; Lafite, P.; Levy, C.; Cheesman, M. R.; Mast, N.; Pikuleva, I. A.; Leys, D.; Munro, A. W. *J. Biol. Chem.* **2009**, *284*, 35524.
(19) Ouellet, H.; Guan, S.; Johnston, J. B.; Chow, E. D.; Kells, P. M.; Burlingame, A. L.; Cox, J. S.; Podust, L. M.; de Montellano, P. R. *Mol. Microbiol.* **2010**, *77*, 730.
(20) Rylott, E. L.; Jackson, R. G.; Edwards, J.; Womack, G. L.; Seth-Smith, H. M.; Rathbone, D. A.; Strand, S. E.; Bruce, N. C. *Nat. Biotechnol.* **2006**, *24*, 216.
(21) Seth-Smith, H. M.; Edwards, J.; Rosser, S. J.; Rathbone, D. A.; Bruce, N. C. *Appl. Environ. Microbiol.* **2008**, *74*, 4550.
(22) Rittle, J.; Green, M. T. *Science* **2010**, *330*, 933.
(23) Groves, J. T.; McClusky, G. A. *J. Am. Chem. Soc.* **1976**, *98*, 859.
(24) Meunier, B.; de Visser, S. P.; Shaik, S. *Chem. Rev.* **2004**, *104*, 3947.
(25) Jung, C.; de Vries, S.; Schunemann, V. *Arch. Biochem. Biophys.* **2011**, *507*, 44.
(26) Dawson, J. H. *Science* **1988**, *240*, 433.
(27) Dey, A.; Jiang, Y.; Ortiz de Montellano, P. R.; Hodgson, K. O.; Hedman, B.; Solomon, E. I. *J. Am. Chem. Soc.* **2009**, *131*, 7869.
(28) Poulos, T. L. *J. Biol. Inorg. Chem.* **1996**, *1*, 356.
(29) Akhtar, M.; Calder, M. R.; Corina, D. L.; Wright, J. N. *Biochem. J.* **1982**, *201*, 569.
(30) Stevenson, D. E.; Wright, J. N.; Akhtar, M. *J. Chem. Soc., Perkin Trans. 1* **1988**, 2043.
(31) Shyadehi, A. Z.; Lamb, D. C.; Kelly, S. L.; Kelly, D. E.; Schunck, W. H.; Wright, J. N.; Corina, D.; Akhtar, M. *J. Biol. Chem.* **1996**, *271*, 12445.
(32) Pikuleva, I. A.; Bjorkhem, I.; Waterman, M. R. *Arch. Biochem. Biophys.* **1997**, *343*, 123.
(33) Omura, T.; Sato, R. *J. Biol. Chem.* **1964**, *239*, 2379.
(34) Sivaramakrishnan, S.; Ouellet, H.; Du, J.; McLean, K. J.; Medzihradszky, K. F.; Dawson, J. H.; Munro, A. W.; Ortiz de Montellano, P. R. *Biochemistry* **2011**, *50*, 3014.
(35) Appleby, C. A.; Blumberg, W. E.; Peisach, J.; Wittenberg, B. A.; Wittenberg, J. B. *J. Biol. Chem.* **1976**, *251*, 6090.
(36) Byrn, M.; Calvin, M. *J. Am. Chem. Soc.* **1966**, *88*, 1916.
(37) Fischer, R. T.; Trzaskos, J. M.; Magolda, R. L.; Ko, S. S.; Brosz, C. S.; Larsen, B. *J. Biol. Chem.* **1991**, *266*, 6124.
(38) Hackett, J. C.; Brueggemeier, R. W.; Hadad, C. M. *J. Am. Chem. Soc.* **2005**, *127*, 5224.
(39) Sen, K.; Hackett, J. C. *J. Am. Chem. Soc.* **2010**, *132*, 10293.
(40) Jiang, Y.; Sivaramakrishnan, S.; Hayashi, T.; Cohen, S.; Moenne-Loccoz, P.; Shaik, S.; Ortiz de Montellano, P. R. *Angew. Chem.* **2009**, *48*, 7193.
(41) Aldag, C.; Gromov, I. A.; Garcia-Rubio, I.; von Koenig, K.; Schlichting, I.; Jaun, B.; Hilvert, D. *Proc. Natl. Acad. Sci. U.S.A.* **2009**, *106*, 5481.
(42) Hu, S.; Kincaid, J. R. *J. Am. Chem. Soc.* **1991**, *113*, 2843.
(43) Lee-Robichaud, P.; Shyadehi, A. Z.; Wright, J. N.; Akhtar, M. E.; Akhtar, M. *Biochemistry* **1995**, *34*, 14104.
(44) Wertz, D. L.; Sisemore, M. F.; Selke, M.; Driscoll, J.; Valentine, J. S. *J. Am. Chem. Soc.* **1998**, *120*, 5331.
(45) Gantt, S. L.; Denisov, I. G.; Grinkova, Y. V.; Sligar, S. G. *Biochem. Biophys. Res. Commun.* **2009**, *387*, 169.
(46) Vaz, A. D.; Pernecky, S. J.; Raner, G. M.; Coon, M. J. *Proc. Natl. Acad. Sci. U.S.A.* **1996**, *93*, 4644.
(47) Chowdhury, G.; Calcutt, M. W.; Guengerich, F. P. *J. Biol. Chem.* **2010**, *285*, 8031.
(48) Cohen, S.; Kumar, D.; Shaik, S. *J. Am. Chem. Soc.* **2006**, *128*, 2649.
(49) Imai, M.; Shimada, H.; Watanabe, Y.; Matsushima-Hibiya, Y.; Makino, R.; Koga, H.; Horiuchi, T.; Ishimura, Y. *Proc. Natl. Acad. Sci. U.S.A.* **1989**, *86*, 7823.
(50) Pikuleva, I. A.; Puchkaev, A.; Bjorkhem, I. *Biochemistry* **2001**, *40*, 7621.